Discovery of a Large Dust Disk Around the Nearby Star AU Microscopii

Paul Kalas,[1,2]* Michael C. Liu,[3] Brenda C. Matthews[1]

We present the discovery of a circumstellar dust disk surrounding AU Microscopii (AU Mic, GJ 803, HD 197481). This young M star at 10 parsec has the same age and origin as β Pictoris, another nearby star surrounded by a dust disk. The AU Mic disk is detected between 50 astronomical units (AU) and 210 AU radius, a region where dust lifetimes exceed the present stellar age. Thus, AU Mic is the nearest star where we directly observe the solid material required for planet formation. Because 85% of stars are M-type, the AU Mic disk provides new clues on how the majority of planetary systems might form and evolve.

About 15% of nearby main sequence stars exhibit an excess of far-infrared radiation that points to the existence of circumstellar dust grains (*1*). Dust grains have short lifetimes, and their continued presence implies a source of replenishment. The solar system has a disk-like distribution of dust that is continually replenished by the sublimation of comets and collisions between asteroids. Therefore, we infer that similar populations of undetected parent bodies produce dusty debris disks around infrared excess stars. Moreover, evidence for planets can be found by matching density variations in debris disks to theoretical models of how planets gravitationally perturb these disks (*2*–*4*). In effect, circumstellar debris disks are a signpost for the existence of extrasolar planetary systems.

Direct images of debris disks are rare. Starlight reflecting off optically thin debris disks is detected at optical and near-infrared wavelengths in only three cases: β Pictoris, HR 4796A, and HD 141569 (*5*–*7*). In three more cases—Vega, Fomalhaut, and ε Eridani—debris disk structure is seen only at thermal infrared wavelengths (*8*, *9*). β Pic, HR 4796A, and HD 141569 are relatively young [<20 million years (My)] main sequence stars that have the largest disk masses and, therefore, represent the more detectable of the debris disk systems.

β Pic has Galactic space motions in common with two M stars, AU Mic and AT Mic, that have ages ~20 My (*10*). These stars and β Pic may be coeval sister stars that have

separated in space over time due to the small differences in their space motions. At least 17 stars may be members of this group with ages from 8 to 20 My (*11*). AU Mic has substantial infrared excess at 60 μm (*12*, *13*), and recent submillimeter data reveal the presence of cold (40 K) dust, a total dust mass roughly three times smaller than that of β Pic (Table 1), an absence of molecular gas, and a lack of grains within 17 AU of the star (*14*).

We endeavored to directly image circumstellar dust around AU Mic with an optical stellar coronagraph at the University of Hawaii 2.2-m telescope on Mauna Kea, Hawaii (*15*). The stellar coronagraph (fig. S1) produces artificial eclipses of stars by blocking the light at the focal plane with a circular opaque mask suspended by four wires. Instrumental diffracted light is blocked by a Lyot mask in the pupil plane. The net result is significantly enhanced contrast in the regions surrounding bright stars. The imaging camera behind the coronagraph is a Tek 2048 × 2048 charge-coupled device (CCD) with a scale of 0.41″/pixel. All of our data were obtained through a standard broadband *R* filter (λ_c = 647 nm, $\Delta\lambda$ = 125 nm).

We acquired data on 14 and 15 October 2003, with 6.5″ and 9.5″ diameter occulting spots, respectively. We obtained five 240-s and three 300-s images of AU Mic on the first and second nights, respectively. In addition to AU Mic, we observed five other bright stars to check for spurious features, such as diffraction spikes and internal reflections (table S1). A disk-like reflection nebulosity surrounding AU Mic was detected in raw data during both nights of observation and does not match the position angle (PA) (measured east from north), width, or morphology of instrumental diffraction spikes. The image quality as measured by the full-width at half-maximum (FWHM) of field stars was ~1.1″.

Data reduction followed the standard steps of bias subtraction, flat fielding, and sky-subtraction. We then subtracted the stellar point spread function (PSF) to remove excess stellar light from around the occulting spot. We used the real PSFs from other stars observed throughout each night, as well as artificial PSFs. Artificial PSF subtraction is effective for AU Mic because the circumstellar disk is close to edge-on. We extracted the stellar PSF for each image of AU Mic by sampling the image radially in a direction perpendicular to the PA of the disk. We then fit a polynomial to the data and generated an artificial PSF that is a figure of rotation of the polynomial. The PSFs were then scaled and registered to each data frame such that subtraction minimized the residual light in directions perpendicular to the disk beyond the edge of the occulting spot. In general, the different PSF subtractions produce comparable results, with minor differences appearing a few pixels beyond the edge of the occulting spot. To evaluate the uncertainties in our final image, we measured disk properties in four different data sets that represent two nights of observation, each with two different PSF subtraction techniques. The data for β Pic from

Table 1. Star (rows 1 to 8) and disk (rows 9 to 13) properties for AU Mic and β Pic. The stellar parameters for AU Mic are derived from data given by (*10*, *13*, *21*). For β Pic's stellar parameters, we use (*22*) and references therein. The β Pic disk *R*-band surface brightness (SB) at 6″ radius is given in (*16*), whereas its maximum extent is given in (*23*). SB fall-off, value of exponent for a power-law fit to disk *R* band surface brightness fall-off between 6 and 16″ radius. The shallower surface brightness profiles correspond to the NW and NE brightness profiles of AU Mic and β Pic, respectively. The β Pic values are taken from (*16*). τ, the fractional dust luminosity, assuming an optically thin disk, determined by taking the ratio of excess infrared luminosity to stellar bolometric luminosity. The values are obtained from (*14*) and (*1*) for AU Mic and β Pic, respectively. Total dust mass from model fits to the spectral energy distributions taken from (*14*) for AU Mic and (*24*) for β Pic.

	AU Mic	β Pic
Spectral type	M1Ve	A5V
Mass ($M_\odot$)	0.5	1.8
T_{eff} (K)	3500	8200
Luminosity ($L_\odot$)	0.1	8.7
Distance (pc)	9.9	19.3
V (mag)	8.8	3.9
M_V (mag)	8.8	2.4
$V - R$	0.88	0.08
Disk SB (6″)	20.1 ± 0.3	15.4 ± 0.3
SB fall-off	−3.6 to −3.9	−3.8 to −4.1
Max. radius (AU)	210	1835
$\tau = L_{disk}/L_{bol}$	6×10^{-4}	3×10^{-3}
Total dust mass (g)	6.6×10^{25}	2.2×10^{26}

[1]Astronomy Department and Radio Astronomy Laboratory, 601 Campbell Hall, Berkeley, CA 94720, USA. [2]National Science Foundation Center for Adaptive Optics, University of California, Santa Cruz, CA 95064, USA. [3]Institute for Astronomy, 2680 Woodlawn Drive, Honolulu, HI 96822, USA.

*To whom correspondence should be addressed. E-mail: kalas@astro.berkeley.edu

(*16*) discussed below were obtained with the same telescope, coronagraph, and filter and were analyzed using similar techniques.

The reflection nebulosity around AU Mic is consistent with a circumstellar disk seen at a near edge-on viewing geometry (Fig. 1; fig. S2). We detect the disk as far as ~21″ (210 AU) from the star (*17*). This sensitivity-limited value is a lower limit to the true disk outer radius. The inner radius of the detected disk is 5″ (50 AU) and is mainly limited by the radius of the occulting spot and artifacts of the PSF subtraction. The position angles of the two disk midplanes differ by about 6° ± 3° (PA = 124° ± 2° for the SE side and PA = 310° ± 1° for the NW side). A similar, 1.0° to 2.5° offset, called the "wing tilt asymmetry," was measured for the β Pic midplanes (*16*). A symmetric disk can appear to have a wing tilt when the disk axis is tilted to the line of sight and

the scattering phase function is nonisotropic. A model-dependent relation between the observed wing tilt and the intrinsic disk inclination (*16*) suggests that AU Mic disk is inclined 7° to 20° from edge-on. In contrast, the sharp midplane morphology is consistent with model disks that have inclinations no greater than ~5° from edge-on (*18*) (fig. S3). Until higher-resolution data are obtained and analyzed, we adopt a disk inclination of ~5° from edge-on.

Power-law fits to the disk midplanes between 6″ (60 AU) and 16″ (160 AU) radius give indices of −3.6 and −3.9 for the NW and SE extensions, respectively (Fig. 2). These indices are similar to the power-law fits for the NE and SW disk extensions of β Pic (Table 1) (*16*). However, the midplane profiles for β Pic become less steep inward of 100 AU. No such turnover is seen for the AU Mic radial profiles.

The NW midplane of AU Mic also shows a significant enhancement in surface brightness at ~9″ radius from the star (Figs. 1 and 2). This could be due to a background source, but further tests using color, polarization, and proper motion information should be evaluated before excluding a physical connection to AU Mic.

The existence of morphologically similar dust disks around AU Mic and β Pic supports the hypothesis that these are sister stars born at the same time and location. However, the two disks are not twins. The total mass of dust estimated from the spectral energy distributions is 3.3 times greater for β Pic relative to AU Mic (Table 1). The relative brightnesses of the two disks in optical data are consistent with this result. To make the comparison, we imagine placing the β Pic dust disk around AU Mic. In Fig. 2, we include the midplane surface brightness profile for β Pic using data from (*16*) that is scaled by factors which account for the AU Mic heliocentric distance and stellar luminosity. We find that if the disk of β Pic surrounded AU Mic it would be about 1.5 mag arc sec^{-2} brighter than what we measure for the AU Mic disk (Fig. 2). This corresponds to a factor of four greater scattering cross section of β Pic grains relative to AU Mic grains. If we assume that the two disks have exactly the same structure, grain properties, and viewing geometry, then the AU Mic disk requires a dust mass that is four times smaller than that of β Pic. Future observations of disk properties such as the inclination of AU Mic will elucidate the validity of these assumptions, but this result is consistent with the infrared dust luminosity.

The underlying grain properties are also likely to differ due to the weak radiation environment of an M star relative to an A star. AU Mic is 3.6 times less massive than β Pic and 87 times less luminous (Table 1). For the AU Mic disk, the collision time scale at 100 AU radius is 0.2 to 1.8 My assuming a dust optical depth of τ ~ 10^{-3} to 10^{-4}, respectively (fig. S4). At 200 AU, near the outer boundary of the detected disk, the collision time scale is 0.5 to 5.0 Myr. Given an age of 8 to 20 My for AU Mic, most disk particles have undergone at least one collision. However, as objects are shattered into smaller pieces, the radiation pressure force around AU Mic is too weak to remove the fragments (*19*). They can be removed by the system either by joining together to form larger objects or by spiraling into the star by Poynting-Robertson (PR) drag. The PR time scales at 100 AU are 0.2 to 1.8 Gy for 1 to 10 μm particles, respectively—many times longer than the age of the system (*1*). For β Pic, in contrast, grains a few micrometers and smaller are quickly ejected by radiation pressure, and the disk mass diminishes over time (*20*). The AU Mic disk should preserve a larger population of submicrometer-sized grains, and the mass of solid objects observed today should approximate the primordial disk mass. In other words, most of the disk seen

Fig. 1. The disk surrounding AU Mic seen in optical scattered light. North is up, east is left, and each side of this false-color image corresponds to 60 arc sec. The central dark region is produced by the 9.5 arc sec diameter focal plane occulting spot, which is suspended by four wires and completely masks our direct view of the star. This image represents 900 s total integration in the *R* band, and each pixel corresponds to 4 AU at the distance to AU Mic. Residual light evident near the occulting spot edge in the NE-SW direction is attributed to asymmetries in the point-spread function caused by instrumental scattering and atmospheric seeing.
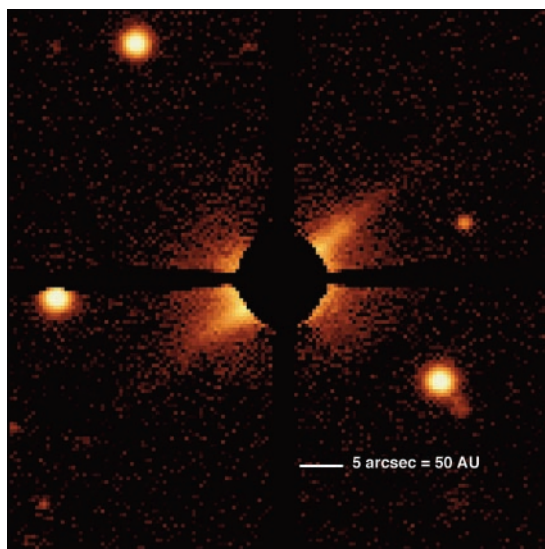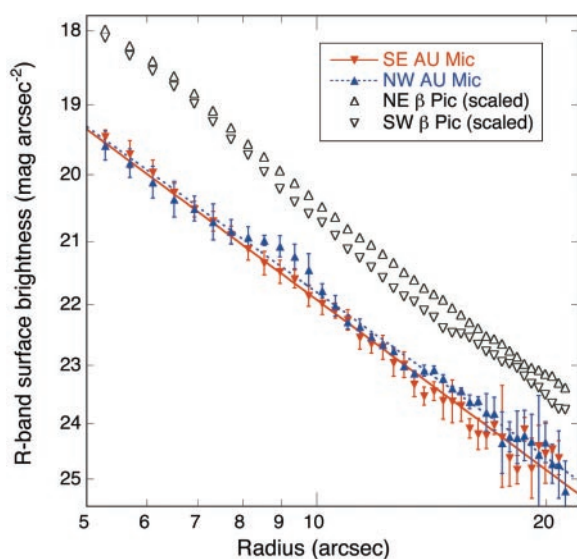
Fig. 2. Midplane surface brightness as a function of radius. The midplane was sampled between 5″ and 21″ radius along a strip 1.2″ wide. We show the mean value from two nights of data with two different PSF subtraction techniques. The error bars represent 1 SD of a single measurement. We fit the data between 6″ and 16″ radius with power laws that give indices −3.6 and −3.9 for the NW and SE midplanes of AU Mic, respectively. The radial profile for the NW midplane has a significant brightness enhancement at ~9″ radius that is either intrinsic to the disk or a background object. We also plot the surface brightness of the β Pic disk from (*16*), but with the surface brightness uniformly 3.0 mag arc sec^{-2} fainter to simulate the existence of β Pic's disk around AU Mic at 9.9 pc. This scaling takes into account the fact that the absolute *R* band magnitude of AU Mic is 5.6 mag fainter than β Pic (Table 1), and at a constant angular radius the β Pic disk is roughly a factor of $(d_{AUMic}/d_{βPic})^{-3.6} = (9.9/19.3)^{-3.6} = 11.3$ times brighter [i.e., 2.6 mag brighter; see Eq. 4 in (*18*)].

in our optical scattered light image may consist of primordial solid material.

Within ~50 AU of the star, the time scales for grain removal by collisions and PR drag become significantly shorter than the stellar age. Primordial dust at the inner limit of our images (Figs. 1 and 2) has mostly vanished, and the grains observed here, as well as those discovered as close as 17 AU from the star (14), must be continually replenished by the collisional erosion of much larger objects such as comets and asteroids. The existence of planetesimals in this region lends plausibility to the argument that the same objects will form planets by accretion. Given that AU Mic is only ~10 My old, we may be able to observe planets that are still in the process of accreting mass, or at least discern disk structure that is sculpted by planet-mass bodies. Because AU Mic is closer to the Sun than β Pic, the 2 to 30 AU zone where terrestrial and gas giant planets might form can be resolved by current and future instrumentation (fig. S5). Planets around AU Mic may also be detected by indirect methods. The low stellar mass means that the star will display a significant astrometric reflex motion (2 milli–arc sec for a Jupiter analog). The near edge-on orientation favors planet detection by transits of the stellar photosphere. Finally, if a planet is detected by radial velocity techniques, then the near edge-on orientation gives the planet mass by constraining the $\sin(i)$ ambiguity intrinsic to these measurements.

References and Notes

1. D. E. Backman, F. Paresce, in *Protostars and Protoplanets III*, E. H. Levy, J. I. Lunine, Eds. (University of Arizona Press, Tucson, 1993), pp. 1253–1304.
2. F. Roques, H. Scholl, B. Sicardy, B. A. Smith, *Icarus* **108**, 37 (1994).
3. J.-C. Liou, H. A. Zook, *Astron. J.* **118**, 580 (1999).
4. L. M. Ozernoy, N. N. Gorkavyi, J. C. Mather, T. A. Taidakova, *Astrophys. J.* **537**, L147 (2000).
5. B. A. Smith, R. J. Terrile, *Science* **226**, 1421 (1984).
6. G. Schneider *et al.*, *Astrophys. J.* **513**, L127 (1999).
7. M. D. Silverstone *et al.*, *Bull. Am. Astron. Soc.* **30**, 1363 (1998).
8. W. S. Holland *et al.*, *Nature* **392**, 788 (1998).
9. J. S. Greaves *et al.*, *Astrophys. J.* **506**, L133 (1998).
10. D. Barrado y Navascues, J. R. Stauffer, I. Song, J.-P. Caillault, *Astrophys. J.* **520**, L123 (1999).
11. B. Zuckerman, I. Song, M. S. Bessell, R. A. Webb, *Astrophys. J.* **562**, L87 (2001).
12. V. Tsikoudi, *Astron. J.* **95**, 1797 (1988).
13. I. Song, A. J. Weinberger, E. E. Becklin, B. Zuckerman, C. Chen, *Astron. J.* **124**, 514 (2002).
14. M. C. Liu, B. C. Matthews, J. P. Williams, P. G. Kalas, *Astrophys. J.*, in press.
15. Materials and methods are available as supporting material on *Science* Online.
16. P. Kalas, D. Jewitt, *Astron. J.* **110**, 794 (1995).
17. To increase the signal-to-noise of the data shown in Fig. 1, we binned the data 3 × 3 pixels and then smoothed by a Gaussian function with σ = 0.5 pixel. This smoothed image was used to find the maximum outer extent of the disk. All other measurements were made using the unbinned and unsmoothed image shown in Fig. 1.
18. P. Kalas, D. Jewitt, *Astron. J.* **111**, 1347 (1996).
19. R. Saija *et al.*, *Mon. Not. R. Astron. Soc.* **341**, 1239 (2003).
20. P. Artymowicz, *Astrophys. J.* **335**, L79 (1988).
21. M. S. Bessel, F. Castelli, B. Plez, *Astron. Astrophys.* **333**, 231 (1998).
22. F. Crifo, A. Vidal-Madjar, R. Lallement, R. Ferlet, M. Gerbaldi, *Astron. Astrophys.* **320**, L29 (1997).
23. J. D. Larwood, P. G. Kalas, *Mon. Not. R. Astron. Soc.* **323**, 402 (2001).
24. W. R. F. Dent, H. J. Walker, W. S. Holland, J. S. Greaves, *Mon. Not. R. Astron. Soc.* **314**, 702 (2000).
25. Supported by the NASA Origins Programme under grant NAG5-11769, and the NSF Center for Adaptive Optics, managed by the University of California at Santa Cruz under cooperative agreement no. AST-9876783. B.C.M. acknowledges support from NSF grant AST-0228963. M.C.L. acknowledges support

Deterministic Generation of Single Photons from One Atom Trapped in a Cavity

J. McKeever, A. Boca, A. D. Boozer, R. Miller, J. R. Buck, A. Kuzmich, H. J. Kimble*

A single cesium atom trapped within the mode of an optical cavity is used to generate single photons on demand. The photon wave packets are emitted as a Gaussian beam with temporal profile and repetition rate controlled by external driving fields. Each generation attempt is inferred to succeed with a probability near unity, whereas the efficiency for creating an unpolarized photon in the total cavity output is 0.69 ± 0.10, as limited by passive cavity losses. An average of 1.4×10^4 photons are produced by each trapped atom. These results constitute an important step in quantum information science, for example, toward the realization of distributed quantum networking.

A crucial building-block for quantum information science is a deterministic source of single photons that generates one-quantum wave packets in a well-controlled spatiotemporal mode of the electromagnetic field. For example, protocols for the implementation of quantum cryptography (1) and of distributed quantum networks (2) rely on this capability, as do models for scalable quantum computation with single-photon pulses as flying qubits (3–6).

The earliest observations of single-photon emission used the fluorescent light from single atoms in two- and three-level configurations (7–9), and thereby produced light with manifestly quantum or nonclassical character. Fluctuations in the number of atoms provided inherent limitations to these original schemes, and have since been mitigated by isolating single ions (10) and molecules (11, 12) and by using individual quantum dots (13, 14) and color centers (15, 16).

With a single dipole, pulsed excitation allows for "triggered" emission of a single photon within a prescribed interval, albeit into 4π steradians. To achieve emission as a directed output with high efficiency, the dipole emitter can be placed

Norman Bridge Laboratory of Physics 12-33, California Institute of Technology, Pasadena, CA 91125, USA.

*To whom correspondence should be addressed. E-mail: hjkimble@caltech.edu

inside an optical resonator, as by coupling single quantum dots to microcavities (17–19). These experiments make use of the Purcell effect to enhance radiative decay into a cavity mode of interest and thereby achieve a deterministic bit stream of single-photon pulses (20) in a regime of weak coupling in cavity quantum electrodynamics (cQED).

By contrast, the generation of single photons within the domain of strong coupling in cQED (21, 22) enables diverse new capabilities, including the reversible transfer of quantum states between atoms and photons as a fundamental primitive for the realization of quantum networks (2). A single photon source consisting of a trapped atom strongly coupled to an optical cavity represents an ideal node for such a network, in which long-lived internal atomic states can be mapped to quantum states of the electromagnetic field by way of "dark" eigenstates of the atom-cavity system (23). By way of a quantum repeater architecture, converting stationary qubits to flying qubits in this way enables distributed quantum entanglement over long distances (2).

We report on the deterministic generation of single-photon pulses by a single atom strongly coupled to an optical cavity in a configuration suitable for quantum network protocols. Single cesium atoms are cooled and loaded into an optical trap (Fig. 1A), which localizes them within the mode of a high-finesse optical cavity (24–26). The atom